Kinetics and Characterization of the Process-Zone Evolution in Polycarbonate

A. KIM,[1] L. V. GARRETT,[2] C. P. BOSNYAK,[3] and A. CHUDNOVSKY[1,*]

[1]Department of Civil Engineering, Mechanics and Metallurgy (M/C 246), University of Illinois at Chicago, P.O. Box 4348, Chicago, Illinois 60680; [2]Wright Laboratory, Aircrew Enclosure Group (WL/FIVR), Wright-Patterson AFB, Ohio 45433-6553; [3]The Dow Chemical Company, Polycarbonate R&D, B-1470, 2301 N. Brazosport Blvd., Freeport, Texas 77541

SYNOPSIS

The process-zone evolution strongly influences the crack growth of polycarbonate. A methodology for determination of the kinetics of the process-zone evolution by decoupling these two processes was developed. This was achieved using constant displacement (stress-relaxation) conditions under which the crack length remained constant. The morphology of the process zone was characterized using optical microscopy of cross sections and fracture surfaces produced with liquid nitrogen. The kinetics of process-zone evolution and stress relaxation were monitored and analyzed. The kinetics vary significantly with the level of displacement imposed. Thus, the challenge remains to construct a master curve for the kinetics. © 1993 John Wiley & Sons, Inc.

INTRODUCTION

Numerous authors have reported that slow-crack propagation in polycarbonate (PC) is commensurate with the formation and growth of a process zone surrounding the crack.[1-4] The energy required for process-zone growth can be many orders of magnitude greater than the surface energy associated with crack formation and, as such, can provide significant resistance to crack growth. Thus, the kinetics of the process-zone development is an essential factor in the PC lifetime determination. However, the kinetics of the process-zone evolution is closely coupled with that of the crack growth, which complicates the determination of the kinetics of the process-zone evolution itself.

The purpose of this study was to develop a methodology for the determination of the kinetics of the process-zone evolution by decoupling these two processes. This is achieved by observing the process-zone growth under stress relaxation at essentially constant crack length. Also presented is a comparative analysis of the mechanism of process-zone formation ahead of the crack with a necking phenomena under simple tensile drawing. In a subsequent paper, we will report the derivation of new constitutive equations for PC process-zone evolution that allow the generation of a master curve for our observations reported here.

* To whom correspondence should be addressed.

Journal of Applied Polymer Science, Vol. 49, 885-892 (1993)
 CCC 0021-8995/93/050885-08

EXPERIMENTAL

(a) Material and Specimen Preparation

Polycarbonate of molecular weight, MW 38,000, Calibre 300-3, was provided by the Dow Chemical Co. in the form of injection-molded plaques of 3 mm thickness. After drying in a vacuum oven at 120°C for 24 h, the plaques were further compressed to 0.7 mm thickness using a Dake compression molder under the following conditions: preheat to 270°C, hold at zero load for 10 min, compression under 4 MN/m^2 for 5 min, then another 8 min under this same compression condition until cooled to 23°C. The single-edge notched (SEN) specimen of dimensions shown in Figure 1(a) and the dogbone specimens [Fig. 1(b)] were machined from the compression-

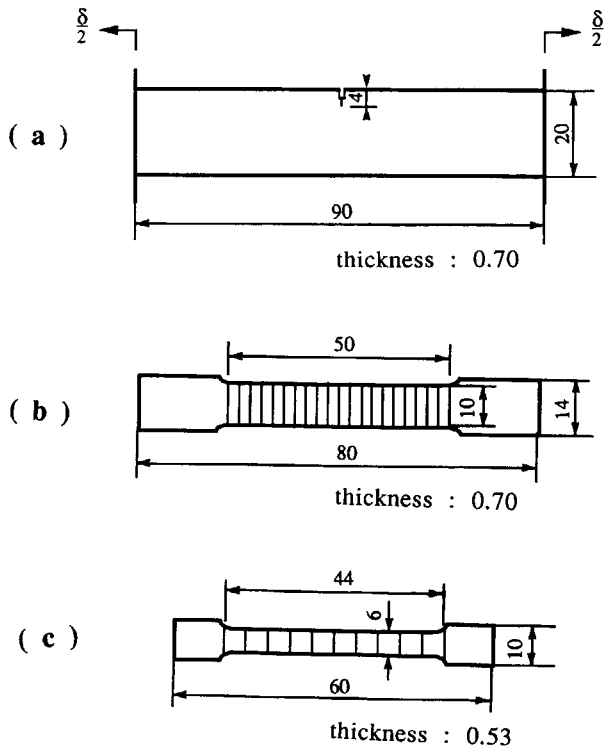

Figure 1 (a) Dimensions of SEN; (b) dogbone specimen for original material; (c) dogbone specimen for drawn material.

molded plaques. The notch tips of SEN specimens were carefully introduced by razor blades. Smaller dogbone specimens, shown in Figure 1(c), were machined from the necked portion of pulled specimens [Fig. 1(b)].

(b) Tensile Test

The dogbone-shaped specimens were marked with horizontal lines [Fig. 1(b)] and pulled at an initial crosshead speed of 0.6 mm/min at 23 ± 1°C. The draw ratio, λ, was determined from the ratio of the spacing between the marked lines of the drawn (necked) material [Fig. 1(c)] to that of the untransformed material. To characterize the properties of the drawn PC, smaller tensile bars with dimensions as shown in Figure 1(c) were cut from the necked region and repulled as above.

(c) Kinetics of Process-Zone Growth under Fixed Displacement

The SEN specimens were strained in tension to fixed displacements, 1.00, 1.15, 1.25, and 1.35 mm, at a constant crosshead speed of 0.6 mm/s at 23 ± 1°C, then held at constant strain. The load was monitored throughout the test. The kinetics of the process-zone evolution was monitored through a video-recording system attached to a microscope. The process-zone size is reconstructed from a combination of a side view from the video screen and optical microscopy of two cross sections perpendicular and parallel to the direction of load application (Fig. 2).

(d) Evaluation of Apparent Shear Band Density

The density of shear bands in the process zone was measured by optical microscopy. A micrograph of a cross section perpendicular to the direction of load application was prepared for the evaluation [Fig. 2(b)]. The shear bands in the micrograph appear to be dark stripes. The micrograph is subdivided into elementary squares, 0.077 × 0.077 mm, and the apparent density of shear bands evaluated as a ratio of the dark stripes inside a unit square to the area of this unit square.

(e) Thinning in the Process Zone

The thinning in the process zone relative to an undeformed region was measured in four specimens using a Zeiss optical microscope with ×200 magnification to an accuracy on the micrometer scale. The thinning was measured at more than 15 sites in each equilibrial process zone to construct the equal thinning level contour (Fig. 11). The thinning is measured as $(z_0 - z)/z_0$, where z is the specimen thickness and z_0 is the undeformed thickness.

RESULTS AND DISCUSSION

Figures 2(a)–(c) are examples of an actual determination of the process-zone shape and size from the side view, cross sections A–A' (normal to the crack plane), and B–B' (surface after fracture in liquid nitrogen). These three projections allow the determination of the process-zone dimensions. It is obvious from Figure 2(b) (cross section A–A') that there is thinning in the thickness direction. In addition, two families of intersecting shear bands are observed. Figure 3 is a schematic of the three-dimensional process zone consisting of intersecting shear bands with varying density. This point will be readdressed later.

Figures 4(a)–(d) show the surfaces of specimens at their equilibrial process-zone state after fracture

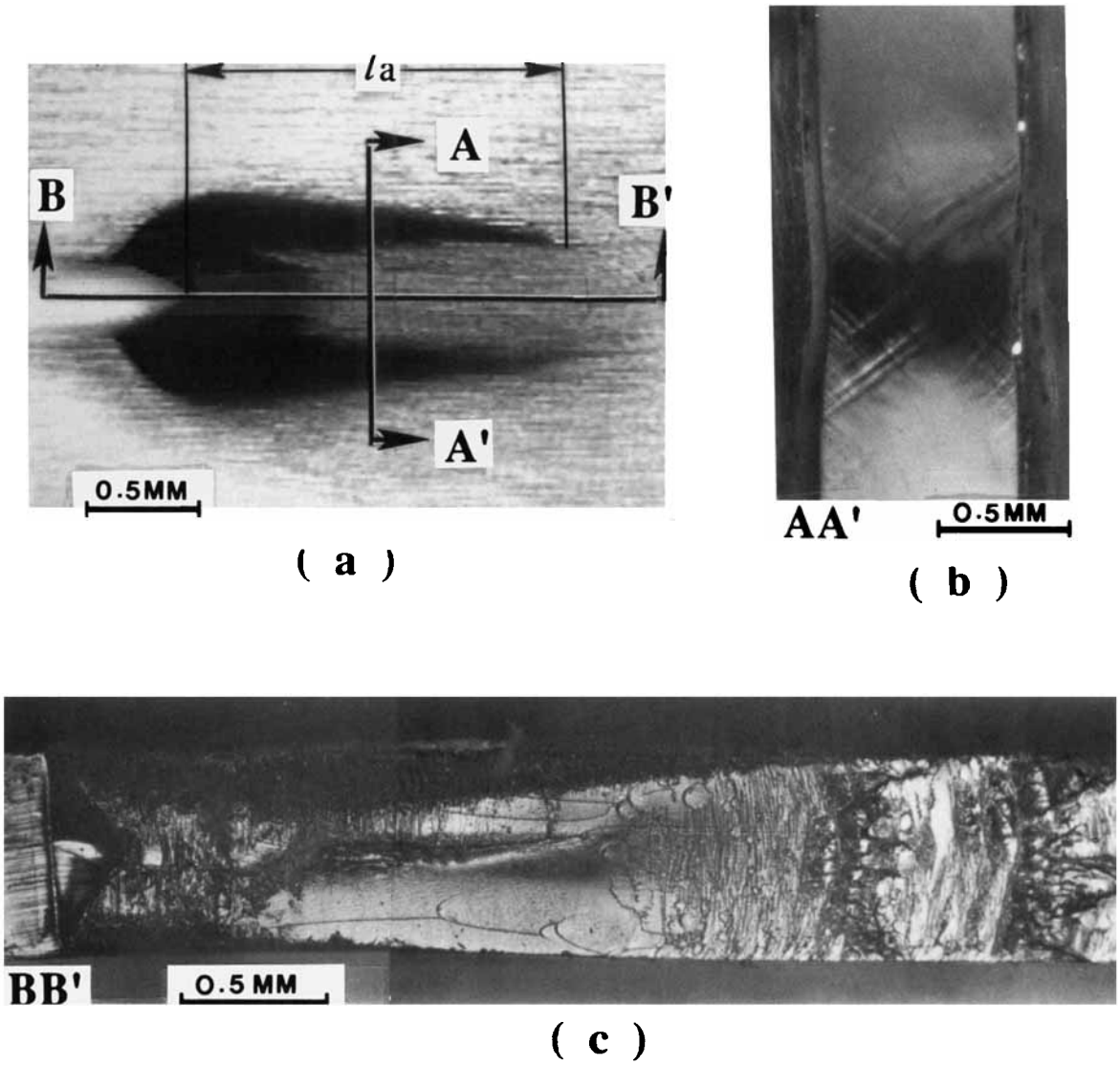

Figure 2 (a) A side view of the process zone from the video screen; (b) cross section A–A' in polarized transmitted light; (c) fracture surface of cross section B–B' fractured in liquid nitrogen.

in liquid nitrogen. The fracture surfaces generated within the process zones are relatively smooth compared to those outside the process zones. The final equilibrial process-zone size is determined based on the side view, thinning profile, and fracture surfaces.

The stress-relaxation behavior during the test is given in Figure 5. The dashed lines indicate the values of remote stress, σ_∞, at an apparent equilibrium. This stress behavior will be utilized in modeling in a subsequent paper.

The kinetics of the process-zone evolution is depicted in Figure 6, which shows the process-zone length, l_a, vs. time for SEN specimens for the four experimental conditions described previously. The process zone is seen to reach at least half of its final length during the initial ramp loading and then follows an increasingly slower approach to an apparent equilibrial size, $l_{a(\mathrm{eq})}$, dependent on the displacement. The dashed lines in Figure 6 represent the values of the equilibrial sizes. Some relatively small crack growth from the notch tip occurred during the initial loading and for a short period thereafter, particularly at the highest strain loading. However, the crack is arrested soon after the stress relaxation starts and remains stationary during subsequent process-zone evolution. Thus, this process occurs at

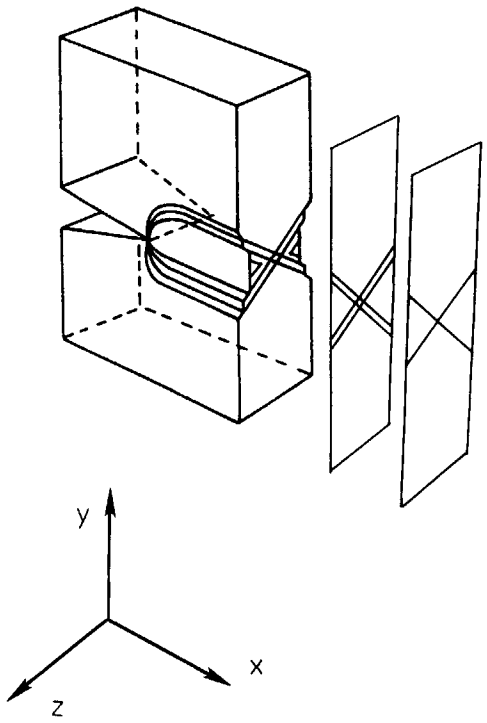

Figure 3 Three-dimensional schematic diagram of the process zone.

essentially constant crack length. Figure 6 represents the process-zone evolution data acquired at this stage.

The rate of the process-zone length, $\dot{l}_a$, evaluated from Figure 6, is shown in Figure 7 as a function of $l_{a(eq)} - l_a$, scaled by the equilibrial length, $l_{a(eq)}$, a measure of the deviation from the equilibrium. The results of four different loading strains apparently show different kinetics. This means that identification of the appropriate scaling factors in the kinetic equations needs to be attempted to develop a master curve.

As described earlier, the process zone consists of two intersecting families of shear bands with orientation $\pm$ 59° with respect to the X–Y plane that are nonhomogeneous in density [see Figs. 2(b) and 3]. The number of shear bands and the bandwidth diminish with distance from the notch along the X-direction. The cumulative effect of the shear bands gives rise to the thinning profile. The gradient of the thinning provides the shadow seen in the side view on the video screen [Fig. 2(a)] and distinguishes the boundary of the process zone and undeformed material.

As described previously in the Experimental section, the relative density of shear bands is obtained from the enlargement of the optical micrograph of Figure 2(b). The contours of equal levels of apparent shear band density is shown in Figure 8. The maximum shear band density corresponds to the plane of the crack. The shape of the contours follows the conventional plastic-zone behavior although there is some asymmetry that may be attributed to the sequence of shear band formation.

Haddaoui et al.[1] drew an analogy of the thinning due to shear band formation in fatigue with necking phenomenon (cold drawing). If this is so, the material properties and formation of shear bands (drawn material) can be estimated separately from the tensile test. In Figure 9, the tensile engineering stress–strain curves are shown for the original undeformed and drawn material. The PC was determined to have Young's modulus of 2.08 GPa, with yield strength, σ_y = 57.7 MPa, followed by necking with constant drawing stress, σ_{dr} = 47.9 MPa until the material in the waist section was exhausted. As is well described elsewhere,[5,6] the transition in the material occurs in a localized zone between the untransformed and transformed regions. The draw ratio was determined as 1.60 for the PC tested here and remained constant throughout the process of neck propagation. The specimens of drawn material showed uniform deformation until fracture with a modulus value of 3.53 GPa, which accounts for the essentially constant value of the draw ratio during the tensile test.

A linear correlation between the apparent average shear band density along the thickness (z direction at y) and the thinning of the thickness (at y) is shown in Figure 10. The data points were measured from Figures 2(b) and 8. The correlation coefficient is .984. Indeed, the linear relationship implies that the integral density of shear bands across the thickness can be evaluated indirectly by measuring the thinning. Though the relationship was examined for one cross section, it can be justified and generalized by the existence of a characteristic slip distance during formation of a shear band, which was observed by Grenet and G'sell.[8]

Based on the above, the thinning in the process zone was measured to evaluate the density of shear bands (drawn material). The equal contour levels of relative thinning in four different equilibrial process zones are shown in Figure 11. Here, the relative thinning is defined by the ratio of the thinning measured in the process zone to the thinning of necked material in the tensile test: $\Delta z(\text{zone})/\Delta z(\text{neck})$. If the density of drawn material in necking is defined as 1, the relative ratio represents the density of shear

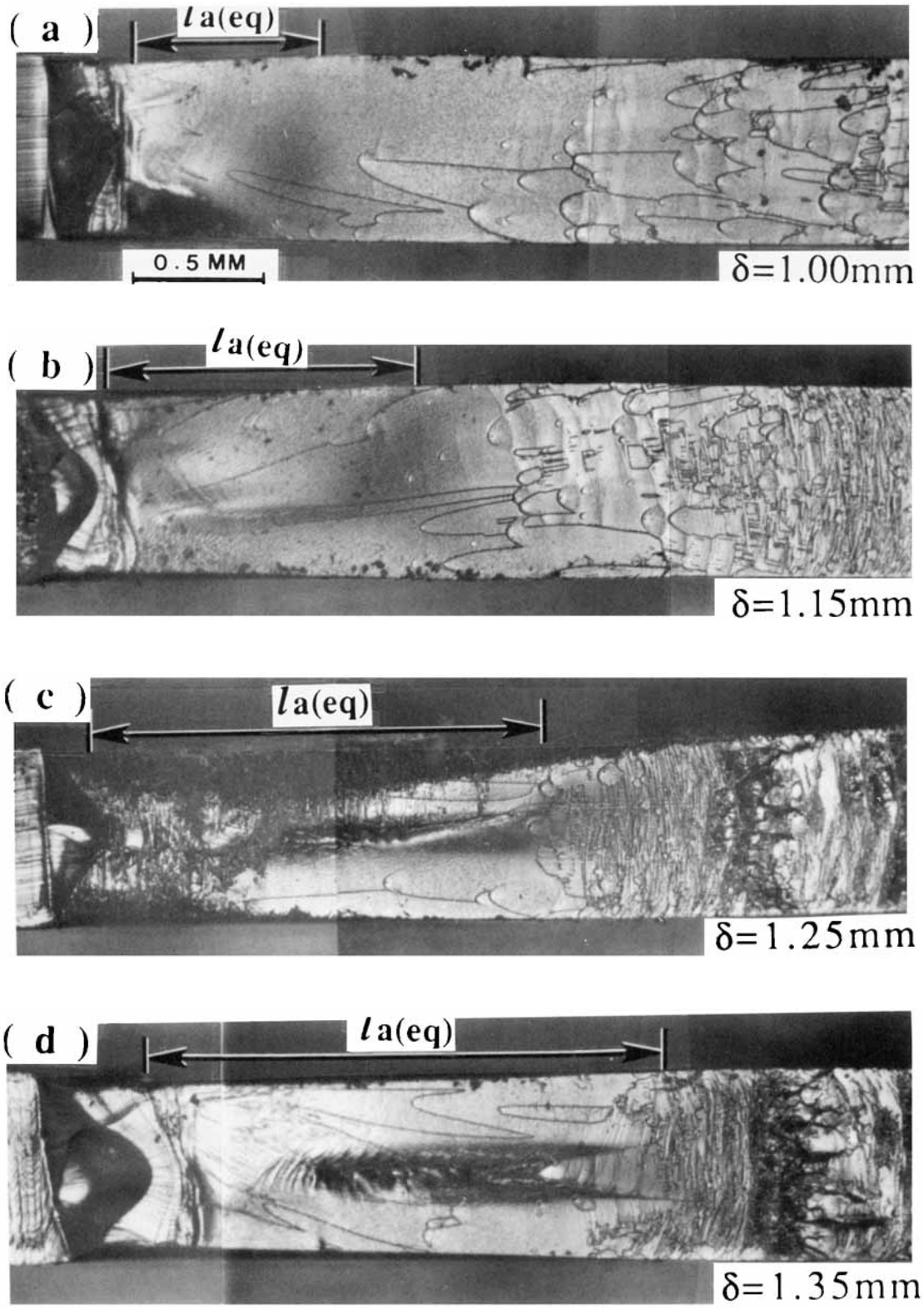

Figure 4 (a)–(d) Fracture surfaces of equilibrium process zones fractured in liquid nitrogen.

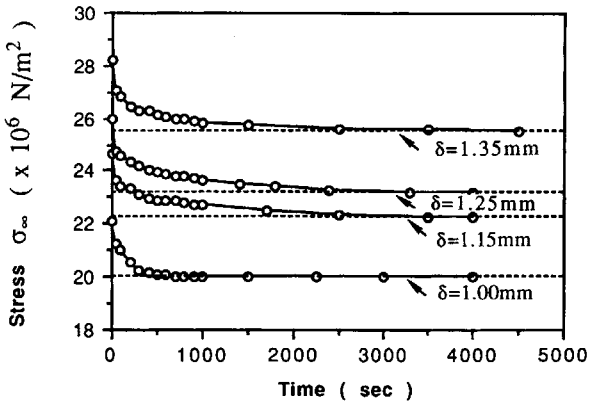

Figure 5 Stress-relaxation data at various displacements in SEN.

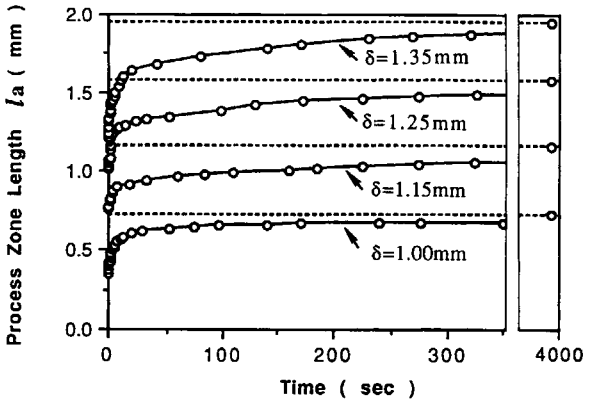

Figure 6 Process-zone length, l_a, vs. time.

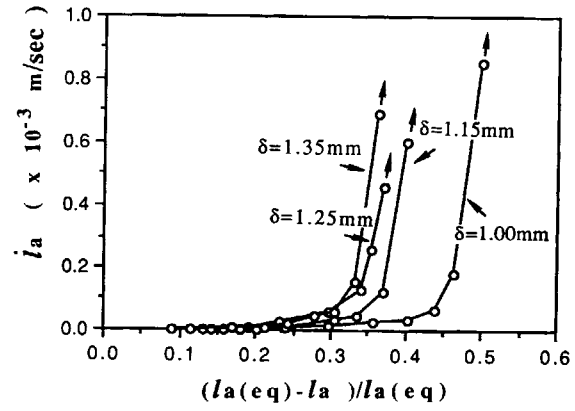

Figure 7 Rate of the process-zone growth, $\dot{l}_a$, vs. $[l_{a(eq)} - l_a]/l_{a(eq)}$.

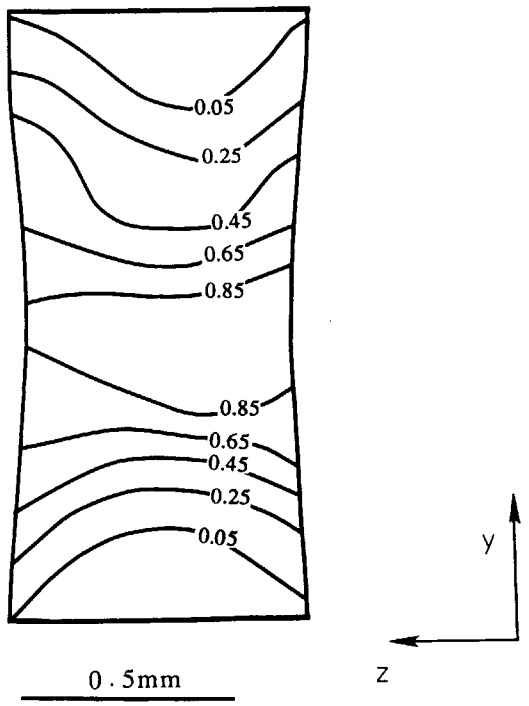

Figure 8 Contour map of apparent shear band density.

bands in the process zone. The average values of this ratio are 0.19, 0.28, 0.35, and 0.35 at load displacements 1.00, 1.15, 1.25, and 1.35 mm, respectively.

SUMMARY

1. An experimental procedure for the study of the kinetics of the process-zone evolution de-

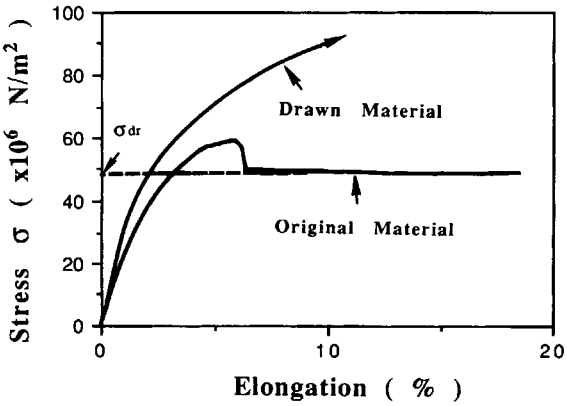

Figure 9 Tensile stress-elongation curves of original and drawn material.

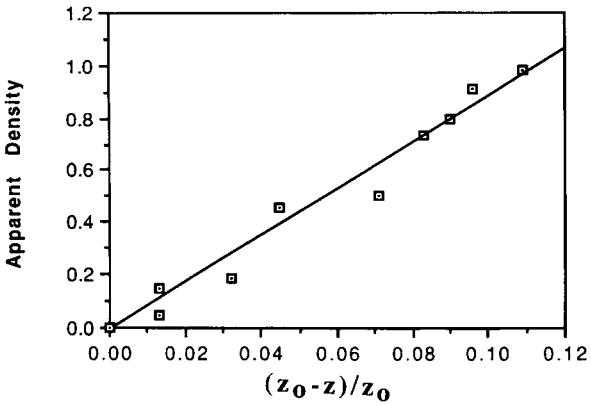

Figure 10 A linear correlation between the apparent average shear band density and the thinning in the process zone.

coupled from the kinetics of crack growth for PC was designed and implemented. This was achieved by observing the process-zone evolution under stress relaxation at essentially constant crack length.

2. The process zone was reconstructed based on the side view, the thinning profile, and liquid nitrogen fracture surface and found to consist of two intersecting families of shear bands with orientation ± 59° with respect to the *X*-*Y* plane and with variable density. The variation of the shear band density was mapped using contour lines of equal relative thinning.
3. The kinetics of the rate of growth of the process-zone length were investigated during stress relaxation. The size and time to reach

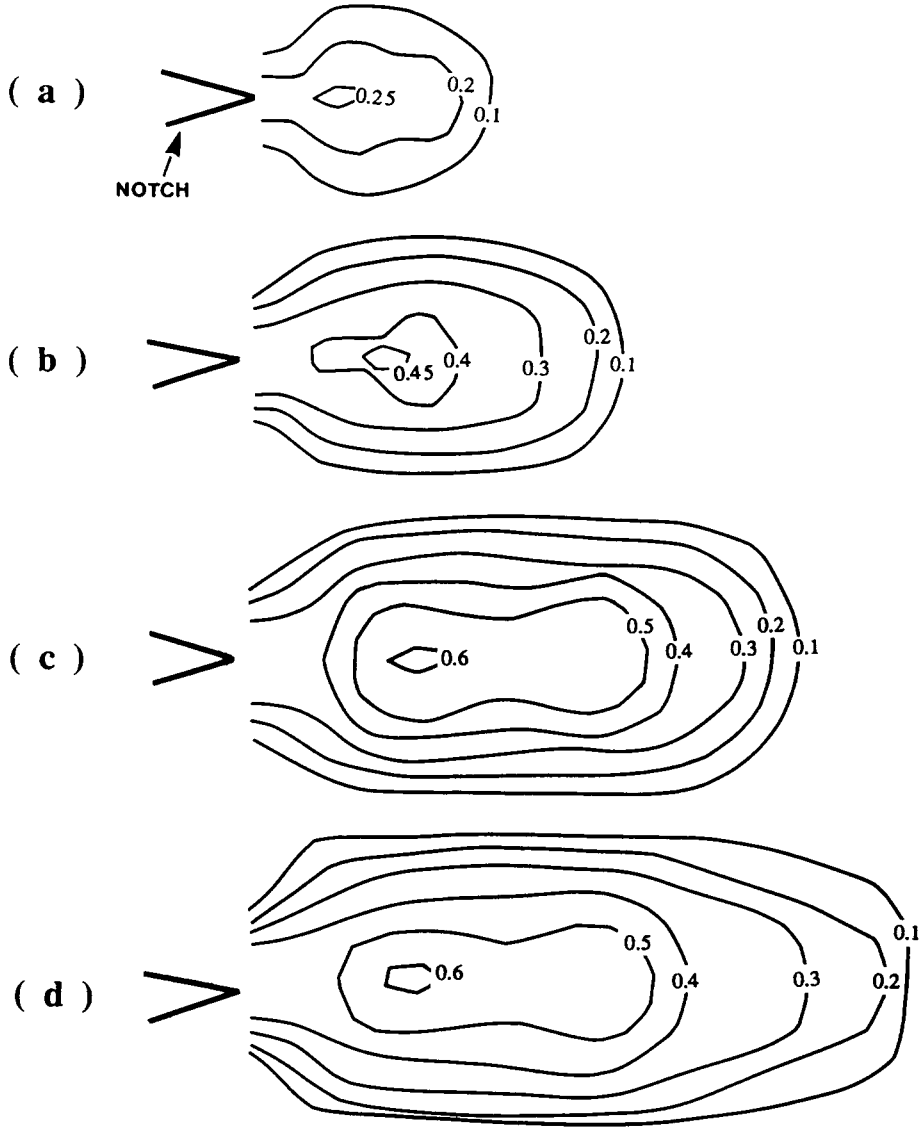

Figure 11 Equal level contours of relative thinning in the process zone.

an equilibrium process zone were dependent on the level of strain imposed.

4. The kinetics of the process-zone evolution was evaluated in terms of the relative deviation of the current process-zone size from its equilibrial value. However, this parameter does not provide adequate scaling. Thus, the challenge remaining is the determination of a suitable parameter to generate a master curve for various experimental conditions.

The financial support from Wright Laboratory provided through the Air Force Office of Scientific Research (Contract No. AFOSR-89-0105) and The Dow Chemical Co. are gratefully acknowledged. Also, Drs. Kalyan Sehanobish and Che-I. Kao, Polycarbonate Research, The Dow Chemical Company, Freeport, Texas, are gratefully acknowledged for their many useful discussions.

REFERENCES

1. N. Haddaoui, A. Chudnovsky, and A. Moet, *Polymer,* **27,** 1377 (1986).
2. A. M. Donald and E. J. Kramer, *J. Mater. Sci.,* **16,** 2967 (1981).
3. H. Nisitani and H. Hyakutake, *Eng. Fract. Mech.,* **22,** 359 (1985).
4. A. Stojimirovic and A. Chudnovsky, to appear.
5. R. N. Haward, Ed., *Physics of Glassy Polymers,* Applied Science, Wiley, New York, 1973.
6. J. W. Maher, R. N. Haward, and J. N. Hay, *J. Polym. Sci.,* **18,** 2169 (1980).
7. M. Ma, K. Vijayan, A. Hiltner, and E. Baer, *J. Mater. Sci.,* **24,** 2687 (1989).
8. J. Grenet and C. G'sell, *Polymer,* **31,** 2057 (1990).
9. G. Buisson and K. Ravi-Chandar, *Polymer,* **31,** 2071 (1990).

Received May 6, 1992
Accepted November 17, 1992